Advanced Safety Range Extension Control System for Electric Vehicle with Front- and Rear-active Steering and Left- and Right-force Distribution

Hiroshi Fujimoto and Hayato Sumiya

***Abstract*— Mileage per charge is a critical issue for electric vehicles. To solve this issue, we have proposed a range-extension control system. Although it is effective for increasing the mileage per charge, it can potentially decrease vehicle stability because a driving force difference between the left and right motors is generated. In this paper, we introduce an advanced safety range-extension control system. The proposed method improves not only the cruise range but also the vehicle stability on a curved road. The effectiveness of the proposed method is verified via experimental results.**

I. INTRODUCTION

Electric vehicles (EVs) are receiving attention because of environmental problems such as global warming, exhaustion of fossil fuels, and air pollution. EVs have excellent potential; they can help alleviate environmental problems as well as allow vehicle motion control because they are driven by electric motors[1]. First, the development of in-wheel motors enables individual control of each wheel. Second, continuous and smooth braking torque can be generated by regeneration. Third, the generated torque can be measured precisely from the motor current. Finally, quick torque response is provided via motor current control. These advantages help achieve effective vehicle motion control[2][3][4].

As described above, EVs have several advantages in terms of environmental performance and vehicle motion control. However, EVs have certain issues that prevent them from becoming widely used. The most critical issue is the mileage per charge. The cruising distance per charge of EVs is very short. To solve this problem, several research efforts have been undertaken to enhance motor efficiency. A variable-parameter permanent-magnet motor was developed in [5] so that magnetic flux can be altered according to the motor speed. Moreover, a novel drive method for the motor was proposed [6], wherein the motor is driven with high efficiency by two reduction gears. However, to solve this problem definitively, it is generally believed that an improvement in battery capacity is necessary.

Our research group has been developing range-extension control systems (RECSs) to enhance the cruising range of EVs by using control technologies [7][8]. Here, "range" refers to the cruising range, which is the distance that can be traveled at a set speed for each charge of the vehicle. If an EV has more than one motor, these control methods can be implemented only by software. In [8], a novel turning method using the yaw-moment generated by the driving force difference between the left and right motors was proposed. When an EV is traveling on a curved road, the yaw-moment is usually generated by the front steering angle only. However, the front steering angle generates not only the yaw-moment but also a cornering resistance. On the other hand, in [8] the yaw-moment is generated by the front steering angle and by the torque difference between the left and right motors. This method can reduce the front steering angle and cornering resistance. As a result, the mileage per charge is improved.

H. Fujimoto and H. Sumiya are with Department of Advanced Energy Graduate School of Frontier Sciences, The University of Tokyo, Chiba 277-8561, Japan fujimoto@k.u-tokyo.ac.jp, sumiya@hflab.k.u-tokyo.ac.jp

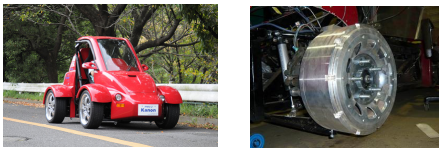

Fig. 1. Experimental vehicle (left) and in-wheel motor (right).

However, this turning method sometimes generates a large vehicle side-slip angle. Moreover, the force generated by one wheel increases because of the torque difference between the left and right motors. As a result, this turning method has the potential to reduce vehicle stability. In this paper, an advanced safety range-extension control system (ASRECS) is proposed. This proposed method integrates the control of the RECS and tire workload equalization [3]. Two control methods are combined into one cost function. The efficiency of the proposed method is investigated via simulation and experiments. Although optimization from the motor output to the yaw-rate and the translational velocity is performed in this paper, the RECS of [8] is also optimized from the battery output to the yaw-rate and the translational velocity.

II. EXPERIMENTAL VEHICLE

An original experimental vehicle called FPEV2-Kanon, which was developed in our laboratory, is used for performance verification. In this section, the characteristics of the experimental vehicle are explained. Four in-wheel motors, which are of the outer-rotor type, are installed in each wheel. Therefore, the vehicle is able to use the yaw-moment generated by the driving force difference between the left and right motors because of the individual control of each wheel. The steering mechanism adopts an active front and rear steering system by using two 250-W DC motors for

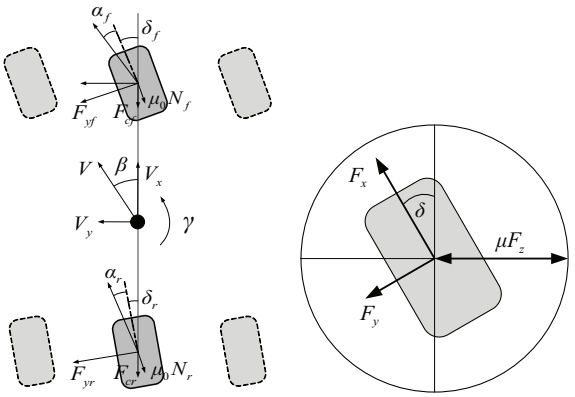

(a) Bicycle model (b) Friction circle

Fig. 2. Vehicle model.

electric power steering (EPS). Moreover, to switch the steer-by-wire and EPS system, the steering wheel shaft has a removable structure. A multi-sensing hub (MSHub) unit is installed in each wheel for measuring the lateral tire force. This is being developed by NSK Ltd. Fig. 1 shows the experimental vehicle.

III. VEHICLE MODELING

A. VEHICLE MODEL

In this section, the vehicle model is explained [9]. Fig. 2(a) shows two vehicle models. The equation for longitudinal motion is represented by

$$M\dot{V} = F_x - F_r,\ F_x := F_{dFL} + F_{dFR} + F_{dRL} + F_{dRR} \quad (1)$$

where F_x is the total driving force, M is the vehicle mass, V is the vehicle velocity, and F_{dij} is the driving force generated by each wheel. i and j are $i = F,\ R$, $j = L,\ R$, for front, rear, left, and right, respectively. Additionally, F_r is the driving resistance term described later. Under the condition that the left and right tire characteristics are the same, each lateral force can be considered as $F_{yFL} \simeq F_{yFR} = F_{yf}$, $F_{yRL} \simeq F_{yRR} = F_{yr}$. Therefore, the vehicle motion can be considered as a simple bicycle model as shown in Fig. 2(a). Lateral motion and yaw dynamics equations are represented by

$$\begin{aligned} MV\left(\dot{\beta} + \gamma\right) &= 2F_{yf} + 2F_{yr}, & (2)\\ I\dot{\gamma} &= 2l_f F_{yf} - 2l_r F_{yr} + N_{zf} + N_{zr}, & (3) \end{aligned}$$

$$N_{zf} := \frac{d_f}{2}\left(-F_{dFL} + F_{dFR}\right),\ N_{zr} := \frac{d_r}{2}\left(-F_{dRL} + F_{dRR}\right),$$

where β is the vehicle side-slip angle, γ is the yaw-rate, I is the vehicle yaw inertia, l_f and l_r are the distances from the body center of gravity to the steering knuckle spindle, and d_f and d_r are the tread bases of the front and rear axles, respectively.

Each lateral force is generated by the front and rear tire side-slip angles α_f and α_r, respectively, which are the angles between the wheel traveling direction and the wheel rotation direction. The tire side-slip angles and lateral forces are represented by

$$\begin{aligned} \alpha_f &= \beta + \frac{l_f\gamma}{V} - \delta_f, & (4)\\ \alpha_r &= \beta - \frac{l_r\gamma}{V} - \delta_r, & (5)\\ F_{yf} &\simeq \frac{-C_f}{\tau s + 1}\alpha_f, & (6)\\ F_{yr} &\simeq \frac{-C_r}{\tau s + 1}\alpha_r, & (7) \end{aligned}$$

where δ_f and δ_r are the front and rear steering angles, respectively, and C_f and C_r are the front and rear cornering stiffnesses, respectively. τ is the time constant of the lateral force generation.

Each vertical load F_{zij} is transferred by the longitudinal and lateral acceleration, and these are represented by

$$\begin{aligned} F_{zFL} &= \frac{1}{2}\frac{l_r}{l}Mg - \rho_f a_y M\frac{h_g}{d_f} - a_x M\frac{h_g}{l}, & (8)\\ F_{zFR} &= \frac{1}{2}\frac{l_r}{l}Mg + \rho_f a_y M\frac{h_g}{d_f} - a_x M\frac{h_g}{l}, & (9)\\ F_{zRL} &= \frac{1}{2}\frac{l_f}{l}Mg - \rho_r a_y M\frac{h_g}{d_r} + a_x M\frac{h_g}{l}, & (10)\\ F_{zRR} &= \frac{1}{2}\frac{l_f}{l}Mg + \rho_r a_y M\frac{h_g}{d_r} + a_x M\frac{h_g}{l}, & (11) \end{aligned}$$

where g is the acceleration of gravity; l is the wheel base; ρ_f and ρ_r are the front and rear distribution ratios of rolling stiffness, respectively; a_x and a_y are the longitudinal and lateral accelerations, respectively; and h_g is the height of the center of gravity.

Additionally, the longitudinal force, lateral force, and vertical load, generated at each wheel, have a relationship to the friction circle as shown in Fig. 2(b). This relationship has to satisfy the equation

$$\sqrt{F_{dij}^2 + F_{yij}^2} \le \mu F_{zij}, \quad (12)$$

where μ is the coefficient of road friction.

B. DRIVING RESISTANCE

Driving resistance is generated when the vehicle is driven on a curved road. It is made up of three elements: rolling friction, cornering resistance generated by front and rear lateral forces, and disturbances such as wind and road conditions. The longitudinal elements of these forces and disturbances become the driving resistance F_r. The driving resistance F_r is represented by

$$\begin{aligned} F_r = {} & 2F_{yf}\sin\delta_f + 2F_{yr}\sin\delta_r + \mu_0(F_{zFL} + F_{zFR})\cos\delta_f \\ & + \mu_0(F_{zRL} + F_{zRR})\cos\delta_r + F_{dis}, \quad (13) \end{aligned}$$

where μ_0 is the coefficient of rolling friction and F_{dis} represents the disturbances such as wind and road slope.

IV. CONTROL SYSTEM DESIGN

A. Range-extension control system

In this section, the cost function of the RECS, minimizing the mechanical output, is defined [8]. In this paper, it is assumed that a front-wheel-drive vehicle has front and rear active steering units. Therefore, the rear driving force is regarded as 0 and $N_{zr} = 0$. The cost function of the RECS is represented by

$$J_{RECS} = T_{FL}\omega_{FL} + T_{FR}\omega_{FR}, \tag{14}$$

where T_{FL} and T_{FR} are the left and right motor torques, respectively, and ω_{FL} and ω_{FR} are left and right wheel angular speeds, respectively. The relationship between the driving force and the yaw-moment N_{zf} is represented by

$$\begin{bmatrix} F_{FL} \\ F_{FR} \end{bmatrix} = \begin{bmatrix} \frac{1}{2} & -\frac{1}{d_f} \\ \frac{1}{2} & \frac{1}{d_f} \end{bmatrix} \begin{bmatrix} F_x \\ N_{zf} \end{bmatrix}, \tag{15}$$

N_{zf} in (3) is regarded as the yaw-moment control input which is generated by the driving force difference between the left and rear motors. Under the condition in which all wheels adhere to the road, the motor torques and driving forces are related as follows:

$$\omega_{FL} = \frac{1}{r}\left(V_x - \frac{d_f}{2}\gamma\right), \tag{16}$$

$$\omega_{FL} = \frac{1}{r}\left(V_x + \frac{d_f}{2}\gamma\right), \tag{17}$$

$$T_{ij} = rF_{dij}, \tag{18}$$

where V_x is the longitudinal vehicle velocity. The cost function J_{RECS} is represented by substituting (15)–(18) for (14),

$$J_{RECS} = F_x V_x + N_{zf}\gamma. \tag{19}$$

Here, it is assumed that the vehicle is running at constant speed. This condition is realized when the total driving force has the same value as the driving resistance: $F_x = F_r$. To derive the cost function J_{RECS}, disturbances such as wind, road slope, and rolling friction of the driving resistance (13) are neglected. The cost function J_{RECS} is represented by

$$J_{RECS} = \left(2F_{yf}\sin\delta_f + 2F_{yr}\sin\delta_r\right)V_x + N_z\gamma. \tag{20}$$

B. Tire workload equalization

In this section, the cost function for the tire workload equalization is defined [3]. Each tire workload ratio η is defined as follows:

$$\eta_{FL} = \frac{\sqrt{F_{dFL}^2 + F_{yf}^2}}{\mu_{\max}F_{zFL}}, \tag{21}$$

$$\eta_{FR} = \frac{\sqrt{F_{dFR}^2 + F_{yf}^2}}{\mu_{\max}F_{zFR}}, \tag{22}$$

$$\eta_{RL} = \frac{\sqrt{F_{dRL}^2 + F_{yRL}^2}}{\mu_{\max}F_{zRL}} \simeq \frac{|F_{yr}|}{\mu_{\max}F_{zRL}}, \tag{23}$$

$$\eta_{RR} = \frac{\sqrt{F_{dRR}^2 + F_{yRR}^2}}{\mu_{\max}F_{zRR}} \simeq \frac{|F_{yr}|}{\mu_{\max}F_{zRR}}, \tag{24}$$

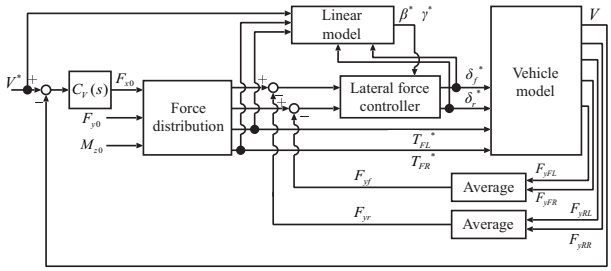

Fig. 3. Block diagram of ASRECS.

where $\mu_{\max}$ is the maximum value of the friction coefficient. Here, we have assumed that the $\mu_{\max}$ values for all the wheels are the same. Next, the cost function J_η is defined. The cost function J_η is the square sum of the workload. J_η is represented by

$$J_\eta = \sum_{i=F,\ R}\sum_{j=R,\ L}\left(\mu_{\max}\eta_{ij}\right)^2. \tag{25}$$

C. Advanced safety range-extension control system

In this section, the construction of the ASRECS is described. The cost function of the ASRECS, J, is defined as

$$J = (1-\nu)\,J_{RECS}W_{RECS} + \nu J_\eta W_\eta, \tag{26}$$

where ν is the distribution ratio, and W_{RECS} and W_η are weighting factors used for normalization. Equation (26) can be minimized by Lagrange's method of undetermined multipliers. To minimize the equation, constraint conditions g_1, g_2, and g_3 are instituted. The constraint conditions are derived from (1)–(3), and the Lagrangian function is represented by

$$L(\boldsymbol{x},\ \lambda) = J + \lambda_1 g_1(\boldsymbol{x}) + \lambda_2 g_2(\boldsymbol{x}) + \lambda_3 g_3(\boldsymbol{x}) \tag{27}$$

$$\boldsymbol{x} = \left[F_{yf}\ F_{yr}\ F_{FL}\ F_{FR}\right]^T, \tag{28}$$

$$\begin{cases} g_1(\boldsymbol{x}) = F_{FL} + F_{FR} - F_{x0}, \\ g_2(\boldsymbol{x}) = 2F_{yf} + 2F_{yr} - F_{y0}, \\ g_3(\boldsymbol{x}) = 2F_{yf}l_f - 2F_{yr}l_r + \frac{d_f}{2}\left(-F_{dFL} + F_{dFR}\right) - M_{z0} \end{cases}$$

where F_{x0} is the total driving force command, F_{y0} is the lateral force command, and M_{z0} is the yaw-moment command. λ_1, λ_2, and λ_3 are constants. It is assumed that β, γ, and V are measurable parameters. Moreover, the front and rear steering angles are considered to be small. In addition, the front and rear steering angles become functions of the tire side-slip angles by substituting (4) and (5) for (27). The tire side-slip angles (4) and (5) are transformed by substituting for steady-state values of (6) and (7). The optimal solutions are derived by Lagrange's method of undetermined multipliers [10].

When the distribution ratio ν is 0.0, this control method becomes a RECS. When the distribution ratio ν is 1.0, this control method becomes a tire workload equalization. When the distribution ratio ν is $0.0 < \nu < 1.0$, this control method becomes an integrated control method. Fig. 3 shows the block diagram of the ASRECS. The optimal solution $\boldsymbol{x}^*$, for which the cost function is minimized, is obtained from

TABLE I

CRUSING RANGE (SIMULATION RESULTS)

Range [km]	ν			
Battery capacity	w/o ctrl	0.0	0.5	1.0
1 kWh	21.0	26.2	24.9	23.2
5 kWh	105	131	125	116
16 kWh	336	419	398	371

the command inputs (F_{x0}, F_{y0}, and M_{z0}). The front and rear steering angle references are generated by a lateral force controller. It is designed to achieve a front and rear lateral force reference of $\boldsymbol{x}^*$. Moreover, the left and right motor torque references are given by

$$T^* = rF_d^* + J_\omega \dot{\omega}. \tag{29}$$

V. SIMULATION

To verify the effectiveness of the proposed method, a simulation is carried out in which the vehicle turns in a steady circle while the vehicle velocity and yaw-rate are kept constant. The simulation parameters used for FPEV2-Kanon are described in Sec. II. The total driving force reference F_{x0} is the output of the vehicle velocity controller, which is designed to compare with results at constant speed. The vehicle velocity controller is designed by using a pole placement method with the plant of (1). The vehicle velocity controller $C_V(s)$ corresponds to the driver model, and the closed-loop pole of this controller is -2 rad/s. The lateral force reference is given by

$$F_{y0} = \frac{MV^2}{R}, \tag{30}$$

where R is the circle radius. In addition, the yaw-moment reference M_{z0} is set to $M_{z0} = 0$. This is because the yaw-rate is constant. The front and rear steering angle references are generated by lateral force controllers. The lateral force controllers, which are a set of proportional and integral controllers, are designed to become multiple roots by the pole placement method with the first-order plant of (6) and (7). The poles of the front and rear lateral force controllers are selected as -3 rad/s and -1 rad/s, respectively. In addition, the references of the front and rear tire side-slip angles are translated into the front and rear steering angles by (4) and (5), respectively. The yaw-rate and the vehicle side-slip angle of (4) and (5) are used for the values calculated in a linear vehicle model [9]. The front and rear cornering stiffnesses, which are used to produce the references of the front and rear steering angles, respectively, are $C_f = 8000$ N/rad and $C_r = 15000$ N/rad, respectively, and the time constant is $\tau = 0.1585$ s.

The conditions of the simulation are as follows: vehicle velocity $V = 15$ km/h and circle radius $R = 6.0$ m. Vehicles without control and with three distribution ratios are examined to verify the effectiveness of the proposed method. The without-control case corresponds to the normal vehicle, and the three distribution ratios are $\nu = 0.0$, $\nu = 0.5$, and $\nu = 1.0$. The distribution ratio $\nu = 0.0$ corresponds to the RECS, the distribution ratio $\nu = 1.0$ corresponds to advanced safety technology of tire work load equalization, and the distribution ratio $\nu = 0.5$ is a collaborative control scheme combining the RECS and advanced safety technology. In addition, the weighting factors W_{RECS} and W_η, used for optimization, are selected to be $W_{RECS} = 2.0 \times 10^{-3}$ and $W_\eta = 1.0$, respectively.

Fig. 4 shows the simulation results. The yaw rates of all methods take almost same values, as shown in Fig. 4(a). However, the side-slip angles vary greatly, as shown in Fig. 4(b). This is because the proposed methods used the rear steering angle and the yaw-moment generated by the driving force difference. Fig. 4(c) shows the vehicle velocity. Vehicle velocities for the proposed methods are higher than that without control. This is because steady-state errors of the vehicle velocity controller become smaller owing to the driving resistance, which decreases when the proposed method is used. The vehicle velocity with a distribution ratio $\nu = 0.0$ is the highest because the driving resistance is minimum in this condition.

Fig. 4(d), Fig. 4(e), and Fig. 4(f) show the front steering angle, the rear steering angle, and the yaw-moment input N_{zf}, respectively. When the proposed method is used, the front steering angle decreases and rear steering angle and the yaw-moment input are used to turn. Fig. 4(h), Fig. 4(i), Fig. 4(j), and Fig. 4(k) show the tire workload ratio for each condition. The tire workload ratio of each wheel is not even when the distribution ratio $\nu = 0.0$. The front steering angle increases and the yaw-moment input N_{zf} decreases with increasing distribution ratio. Fig. 4(g) shows the mechanical output. The mechanical output decreases by 100, 70, and 50 W for distribution ratios of $\nu = 0.0$, $\nu = 0.5$, and $\nu = 1.0$, respectively. As a result, it is confirmed that the distribution ratio $\nu = 0.0$ minimizes the mechanical output, and the distribution ratio $\nu = 1.0$ equalizes the tire workload ratio. Moreover, the distribution ratio $\nu = 0.5$ becomes a collaboration control between RECS and tire workload equalization.

The cruising range (km) per energy (kWh) is evaluated based on these simulations. The energy E is calculated by integrating the mechanical output $T\omega$ over the measurement time t. Here, to calculate it, the motor and inverter efficiencies are neglected and they are assumed to be 100%. Then, in the same manner, the driving distance L is obtained by integrating the vehicle velocity over the same measurement time t. Therefore, by dividing L by E, the cruising range (km) per energy (kWh) can be obtained. The results are listed in Table. I. The battery capacities are assumed to be 5 kWh for our experimental vehicle described in Sec. II and 16 kWh for the i-MiEV produced by Mitsubishi Motors [11]. By comparing with the case without control, we see that improvements of 25%, 18%, and 10% can be achieved for distribution ratios of $\nu = 0.0$, $\nu = 0.5$, and $\nu = 1.0$, respectively.

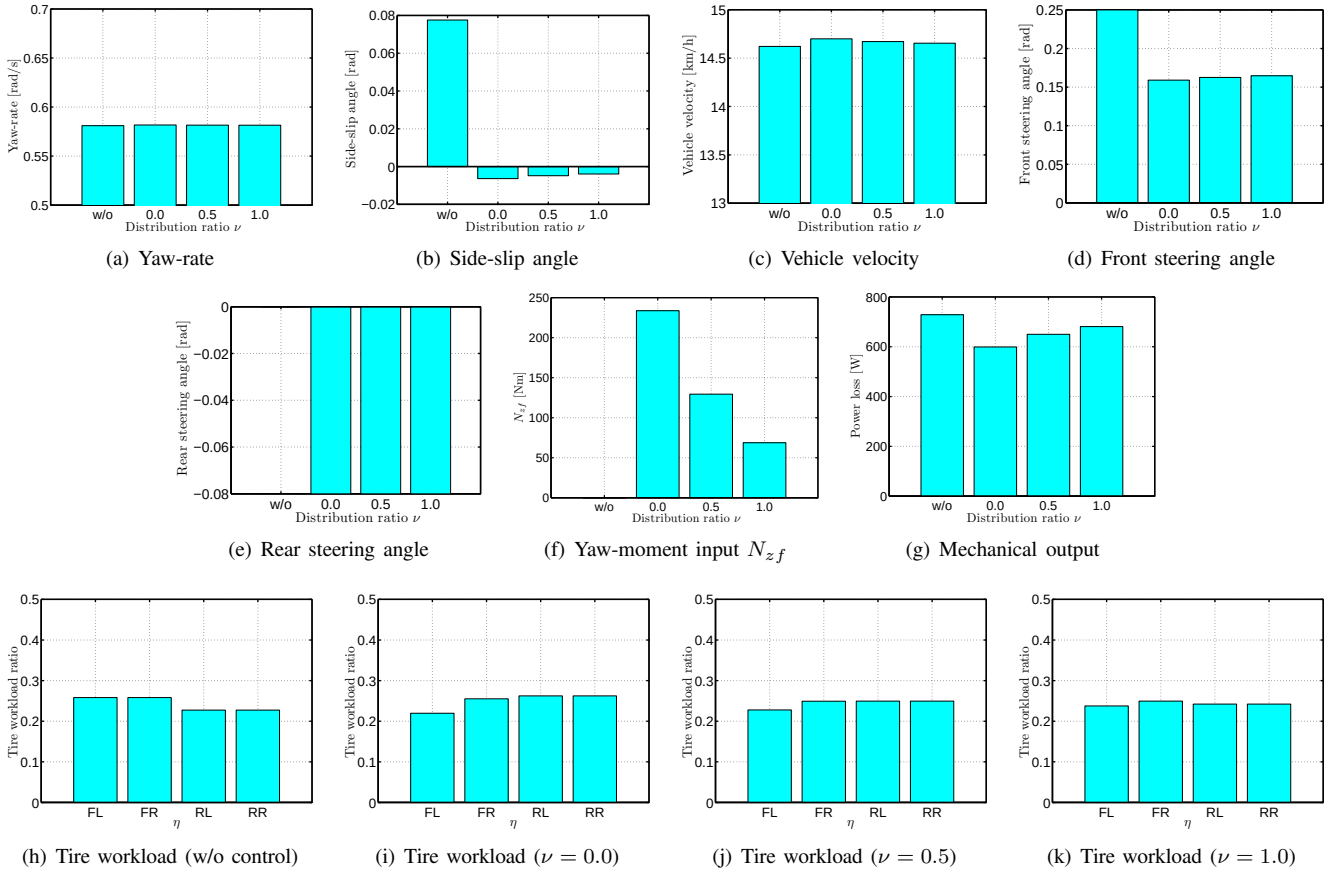

(a) Yaw-rate (b) Side-slip angle (c) Vehicle velocity (d) Front steering angle

(e) Rear steering angle (f) Yaw-moment input N_{zf} (g) Mechanical output

(h) Tire workload (w/o control) (i) Tire workload ($\nu = 0.0$) (j) Tire workload ($\nu = 0.5$) (k) Tire workload ($\nu = 1.0$)

Fig. 4. Simulation results.

VI. EXPERIMENT

The experiments are conducted in conditions similar to those of the simulation. The front lateral force is measured by a lateral force sensor as shown in Sec. II, and the rear lateral force is calculated by (2). The lateral acceleration of (2) is measured using an acceleration sensor. The experimental conditions are as follows: vehicle velocity $V = 15$ km/h and circle radius $R = 6.0$ m. Fig. 5 shows the experimental results.

Fig. 5(a), Fig. 5(b), and Fig. 5(c) show the yaw-rate, the vehicle side-slip angle, and the vehicle velocity. The yaw rates of the case without control and the proposed methods are almost the same. However, the vehicle side-slip angles are different between the without-control case and the proposed methods because of the rear steering angle and the yaw-moment input. The vehicle velocities of the proposed methods are faster than that without control because of the driving resistance decrease. Fig. 5(d), Fig. 5(e), and Fig. 5(f) show the front and rear steering angles and the yaw-moment input N_{zf}. Although without control the vehicle is turned by the front steering angle only, in the proposed method the vehicle is turned by the front and rear steering angles and the yaw-moment input. In addition, the yaw-moment input decreases with an increase in the distribution ratio ν, and the front steering angle increases.

Fig. 5(h)–Fig. 5(k) show the results of the tire workload ratio for each distribution ratio. In $\nu = 0.0$, the tire workload ratio of the rear-left wheels is very high. However, for $\nu = 0.5$ and $\nu = 1.0$, it is confirmed that the tire workloads are equalized by the proposed method. Fig. 5(g) shows the mechanical output, as calculated by (14). Comparing with the case without control, we see that improvements of 6% and 3% can be achieved for the distribution ratios of $\nu = 0.0$ and $\nu = 0.5$, respectively. However, the mechanical output with a distribution ratio of $\nu = 1.0$ is higher than that without control. This is because the distribution ratio $\nu = 1.0$ corresponds to advanced safety.

Table. II lists the cruising range (km) per energy (kWh). These lists are calculated in a manner similar to that used for the simulation. Comparing with the case without control, we see that improvements of 8% and 5% can be achieved for the distribution ratios of $\nu = 0.0$ and $\nu = 0.5$, respectively. The cruising range per energy with a distribution ratio $\nu = 1.0$ is almost the same as that without control.

VII. CONCLUSION

In this paper, an advanced safety range-extension control system is proposed and the efficiency of the proposed method is confirmed via a simulation and experiment. Future work will involve examining another turning method and considering electrical loss.

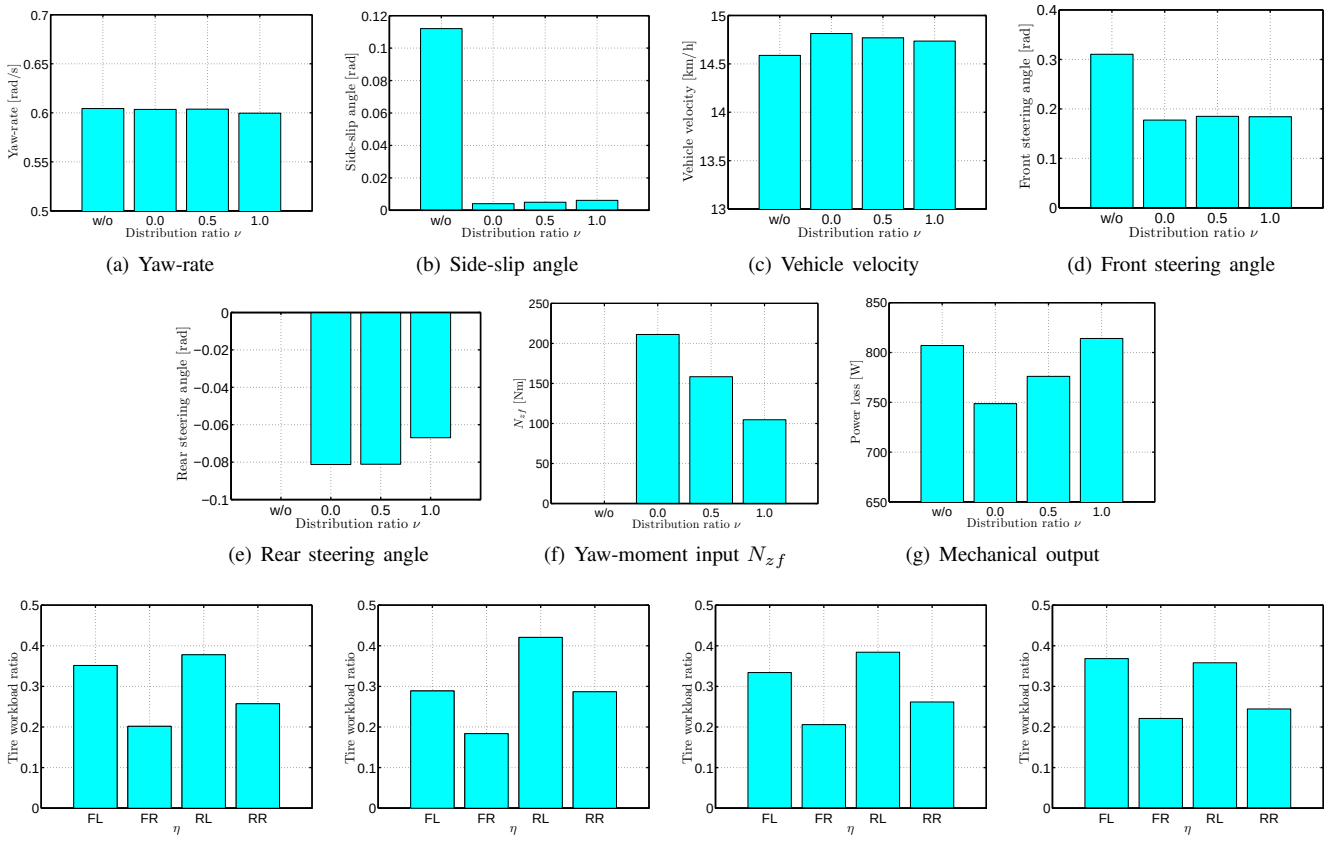

(a) Yaw-rate (b) Side-slip angle (c) Vehicle velocity (d) Front steering angle

(e) Rear steering angle (f) Yaw-moment input N_{zf} (g) Mechanical output

(h) Tire workload (w/o control) (i) Tire workload ($\nu = 0.0$) (j) Tire workload ($\nu = 0.5$) (k) Tire workload ($\nu = 1.0$)

Fig. 5. Experimental results.

TABLE II
CRUSING RANGE (EXPERIMENTAL RESULTS)

Range [km]	ν			
Battery capacity	w/o ctrl	0.0	0.5	1.0
1 kWh	18.1	19.8	19.0	18.1
5 kWh	90.5	99.0	95.0	90.5
16 kWh	289.6	316.8	304.0	289.6

VIII. ACKNOWLEDGMENTS

This research was partly supported by the Industrial Technology Research Grant Program from the New Energy and Industrial Technology Development Organization (NEDO) of Japan and in part by the Ministry of Education, Culture, Sports, Science and Technology (Grant number 22246057). The authors would like to thank NSK Ltd., for providing a MSHub unit.

REFERENCES

[1] Y. Hori, "Future vehicle driven by electricity and control—research on four-wheel-motored 'UOT electric march II'," *IEEE Transactions Industrial Electronics*, vol. 51, no. 5, pp. 954–962, 2004.

[2] H. Fujimoto, "Regenerative brake and slip angle control of electric vehicle with in-wheel motor and active front steering," in *Proceedings 1st International Electric Vehicle Technology Conference*, no. 20117205, 2011.

[3] N. Ando and H. Fujimoto, "Yaw-rate control for electric vehicle with active front/rear steering and driving/braking force distribution of rear wheels," in *11th IEEE International Workshop on Advanced Motion Control Proceedings*, pp. 726–731, 2010.

[4] S. Murata, "Vehicle dynamics innovation with in-wheel motor," in *Proceedings 1st International Electric Vehicle Technology Conference*, no. 20117204, 2011.

[5] K. Sakai, K. Yuki, Y. Hashiba, N. Takahashi, and K. Yasui, "Principle of the variable-magnetic-force memory motor," in *Proceedings International Conference of Electrical Machines and Systems*, pp. 978–1–4244–5177–7, 2009.

[6] A. Sorniotti, M. Boscolo, A. Turner, and C. Cavallino, "Optimisation of a 2-speed gear box for an electric vehicle," in *Proceedings 10th International Symposium on Advanced Vehicle Control*, pp. 755–760, 2010.

[7] H. Fujimoto and H. Sumiya, "Range extension control system of electric vehicle based on optimal torque distribution and cornering resistance minimization," in *Proceedings of the 37th Annual Conference of the IEEE Industrial Electronics Society*, pp. 3727–3732, 2011.

[8] H. Sumiya and H. Fujimoto, "Distribution method of front/rear wheel side-slip angles and left/right motor torques for range extension control system of electric vehicle on curving road," in *Proceedings 1st International Electric Vehicle Technology Conference*, no. 20117208, 2011.

[9] R. Rajamani, *Vehicle Dynamics and Control*. Springer Science & Business Media, 2006.

[10] H. Sumiya and H. Fujimoto, "Proposal of Advanced Safty Range Extension Control System for Electric Vehicle Based on Front?Rear Lateral Force Control and Driving/Braking Force Control" in *JSME Translog*, no. 3102, pp. 171–174, 2011 (in Japanese).

[11] M. Kamachi, H. Miyamoto, and H. Yoshida, "Development of electric vehicle for on-road test," in *Proceedings 8th International Symposium on Advanced Vehicle Control*, pp. 665–669, 2008.